

Long-Tailed 3D Detection via 2D Late Fusion

Yechi Ma^{12*}, Neehar Peri^{3*}, Shuoquan Wei², Wei Hua², Deva Ramanan³, Yanan Li², Shu Kong⁴⁵

¹Zhejiang University, ²Zhejiang Lab, ³Carnegie Mellon University, ⁴University of Macau, ⁵Texas A&M University

Abstract

Autonomous vehicles (AVs) must accurately detect objects from both common and rare classes for safe navigation, motivating the problem of Long-Tailed 3D Object Detection (LT3D). Contemporary LiDAR-based 3D detectors perform poorly on rare classes (e.g., CenterPoint only achieves 5.1 AP on stroller) as it is difficult to recognize objects from sparse LiDAR points alone. RGB images provide visual evidence to help resolve such ambiguities, motivating the study of RGB-LiDAR fusion. In this paper, we delve into a simple late-fusion framework that ensembles independently trained RGB and LiDAR detectors. Unlike recent end-to-end methods which require paired multi-modal training data, our late-fusion approach can easily leverage large-scale uni-modal datasets, significantly improving rare class detection. In particular, we examine three critical components in this late-fusion framework from first principles, including whether to train 2D or 3D RGB detectors, whether to match RGB and LiDAR detections in 3D or the projected 2D image plane, and how to fuse matched detections. Extensive experiments reveal that 2D RGB detectors achieve better recognition accuracy than 3D RGB detectors, matching on the 2D image plane mitigates depth estimation errors, and fusing scores probabilistically with calibration leads to state-of-the-art LT3D performance. Our late-fusion approach achieves 51.4 mAP on the established nuScenes LT3D benchmark, improving over prior work by 5.9 mAP.

1. Introduction

3D object detection is an integral component of the autonomous vehicle (AV) perception stack [3, 14]. To foster 3D perception research, the AV industry has released numerous large-scale multi-modal datasets [3, 52, 61]. However, despite significant improvement in detecting common classes like car and bus, state-of-the-art detectors still perform poorly on rare classes like stroller and

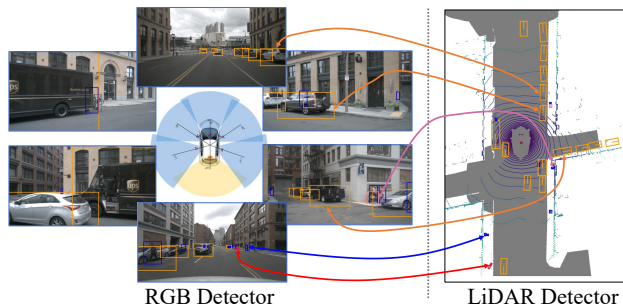


Figure 1. We explore a simple late-fusion framework for LT3D by ensembling RGB and LiDAR uni-modal detectors [42]. We rigorously examine three critical components (Fig. 2) from first principles and propose a simple method that fuses detections produced by 2D RGB and 3D LiDAR detectors. Our method achieves 51.4 mAP on the nuScenes [3] LT3D benchmark, significantly outperforming prior work [39] by 5.9 mAP (cf. Table 1).

debris, which can impact downstream planning, motivating the study of Long-Tailed 3D Detection (LT3D) [42].

Status Quo. Long-Tailed 3D Detection cannot be solved simply by training state-of-the-art (SOTA) detectors on both common and rare classes [42]. For example, BEVFusion [39], an end-to-end trained multi-modal transformer-based detector, only achieves 4.4 AP on the rare class child. In contrast, [42] finds that late-fusion of monocular 3D RGB detections [57] and 3D LiDAR detections [66] improves rare class recognition (cf. Fig. 1), achieving SOTA performance on the nuScenes [3] LT3D benchmark. Importantly, [42] shows that (a) 3D LiDAR detectors achieve high recall but struggle to correctly recognize rare objects, and (b) RGB detectors are better at recognition but are unable to reliably estimate depth.

Technical Insights. To address LT3D, we delve into the simple late-fusion framework proposed by [42] (cf. Fig. 1) and study three critical design choices from first principles (cf. Fig. 2), including whether to train 2D or 3D RGB detectors, whether to match RGB and LiDAR detections in the 2D image plane or 3D bird’s-eye-view, and how to fuse matched detections.

First, we evaluate the impact of using 2D versus 3D RGB detectors for late-fusion, and find that the former is straightforward to train, can readily leverage external datasets that

* The first two authors equally contributed to this work.

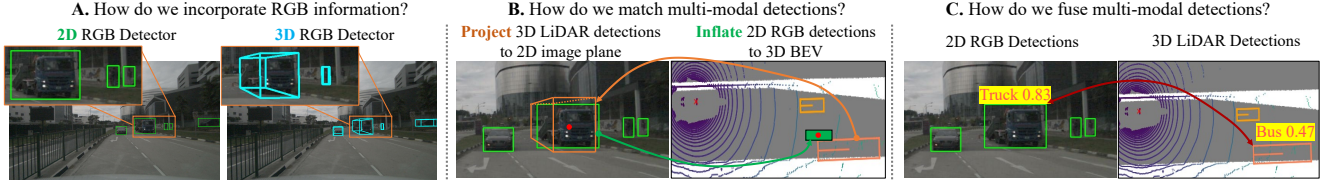


Figure 2. We examine three key components in the late-fusion of uni-modal RGB and LiDAR detectors: **A.** whether to train 2D or 3D monocular RGB detectors, **B.** whether to match uni-modal detections on the 2D image plane or in the 3D bird’s-eye-view (BEV), and **C.** how to optimally fuse matched detections. Perhaps surprisingly, our exploration reveals that using 2D RGB detectors, matching on the 2D image plane, and combining calibrated scores with Bayesian fusion yields state-of-the-art LT3D performance, significantly outperforming end-to-end trained multi-modal detectors (cf. Table 1).

have 2D annotations, and leads to higher AP averaged over all classes. This is practically meaningful because annotating 2D boxes on RGB images is significantly cheaper than annotating 3D cuboids.

Next, we study the impact of matching 2D RGB detections and 3D LiDAR detections on the 2D image plane versus in the 3D bird’s-eye-view (BEV). Matching detections in the 3D BEV requires inflating 2D detections to 3D using depth imputed from LiDAR points [59]. This introduces additional depth estimation errors. Instead, we demonstrate that projecting 3D LiDAR detections to the 2D image plane for matching is more robust.

Lastly, we explore score calibration and Bayesian fusion to combine matched detections. We find that proper score calibration improves rare class detection and enables probabilistic fusion [8] of LiDAR and RGB detections. Without score calibration, rare class detections are often suppressed by overlapping common class detections.

Contributions. We make three major contributions:

1. We extensively study three design choices within the late-fusion framework (Fig. 2), and draw technical insights that generalize across detector architectures.
2. Motivated by the above study, we present a simple late-fusion approach that effectively fuses 2D RGB-based detections and 3D LiDAR-based detections.
3. We conduct comprehensive experiments to ablate our design choices and demonstrate that our simple method achieves state-of-the-art results on the nuScenes and Argoverse 2 LT3D benchmarks.

2. Related Work

3D Detection for Autonomous Vehicles (AVs) can be broadly classified based on input modalities: LiDAR-only, RGB-only, and multi-modal detectors. Recent work in 3D detection is inspired by prior work in 2D detection [5, 38, 72]. LiDAR-based detectors like PointPillars [30], CBGS [74], and PVRCNN++ [51] adopt an SSD-like architecture [38] that regresses amodal bounding boxes from a BEV feature map. More recently, CenterPoint [66] adopts a center-regression loss that is inspired by [72]. Despite significant progress, LiDAR-based detectors often produce

many false positives because it is difficult to distinguish foreground objects from background with sparse LiDAR points alone. On the other hand, monocular RGB-based methods have gained increased interest in recent years due to low sensor cost and wide-spread adoption [22]. FCOS3D [57] extends FCOS [54] by additionally regressing the size, depth, and rotation for each detection. Recent methods such as BEVDet and BEVFormer [24, 25, 34] construct a BEV feature-map by estimating per-pixel depth [44]. PolarFormer [27] introduces a polar-coordinate transformation that improves near-field detection. Importantly, many of these state-of-the-art 3D RGB detectors are commonly pre-trained on large external datasets like DDAD [16]. Monocular RGB detectors accurately classify objects but struggle to estimate depth, particularly for far-field detections [19]. Despite recent advances in LiDAR and RGB 3D detectors, we find that multi-modal fusion is essential for LT3D (detailed next). Importantly, using both RGB (for better recognition) and LiDAR (for better 3D localization) helps detect rare classes. We delve into the late-fusion framework described in Fig. 1 to determine how to effectively fuse RGB and LiDAR uni-modal detectors for LT3D (cf. Fig. 2).

Multimodal Fusion for 3D Object Detection is an active area of research. Popular approaches can be categorized into input-fusion, feature-fusion, and late-fusion. Input-fusion methods typically augment LiDAR points using image-level features. For example, PointPainting [55] projects LiDAR points onto a semantic segmentation mask and appends corresponding class scores to each point. MVP [67] densifies regions of LiDAR sweeps that correspond with objects in semantic segmentation masks. Frustum PointNets [45] and SRDL [21] leverage 2D RGB detections to regress 3D bounding boxes for LiDAR points within the 2D detection frustum using PointNets [46]. Recent works show that feature-fusion can be more effective than input-fusion. PointFusion [62] fuses global image and point-cloud features prior to detection and MSMDFFusion [28] fuses LiDAR and RGB features at multiple scales. [35] proposes a multi-task network that reasons about 2D and 3D object detection, ground estimation and depth completion. TransFusion [2] and BEVFusion [39] fuse features in the BEV space using multi-headed attention. Despite the

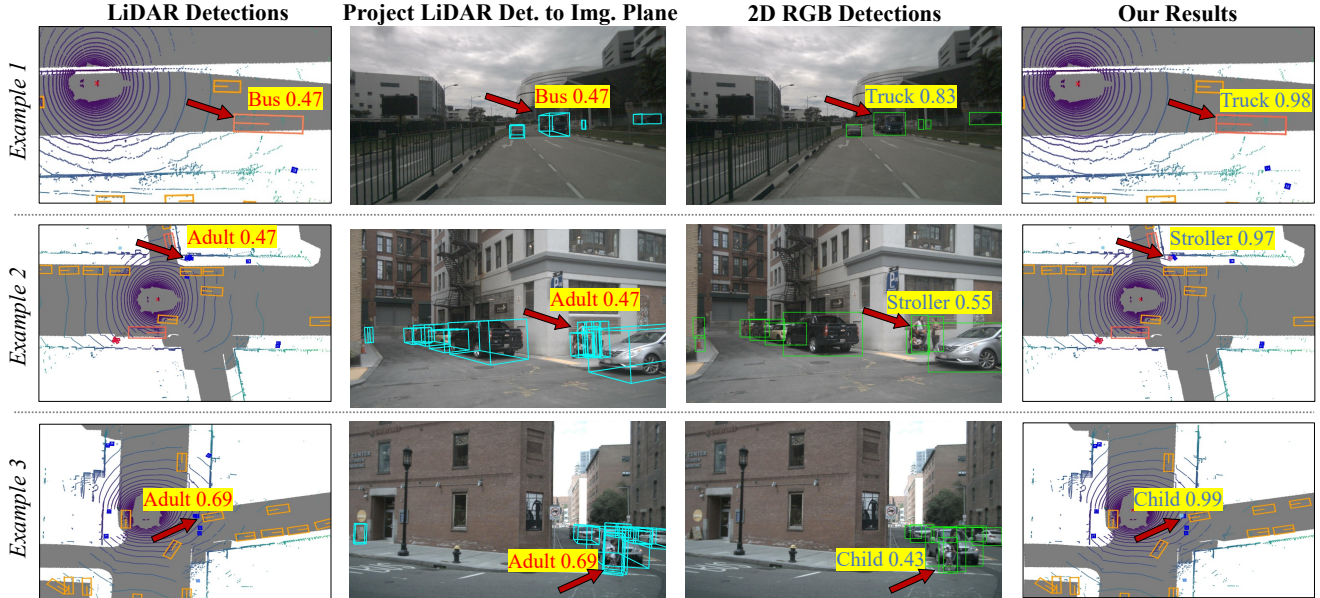


Figure 3. We highlight three examples to demonstrate how ensembling 2D RGB detections from DINO and 3D LiDAR detections from CenterPoint improves LT3D performance. In all examples, our method is able to correctly relabel detections which are geometrically similar (e.g., size and shape) in LiDAR but visually distinct in RGB, such as bus-vs-truck, adult-vs-stroller, and adult-vs-child. In addition, our method adopts probabilistic score fusion to boost confidence scores.

success of transformers for detecting common objects, [42] finds that TransFusion struggles to detect rare classes, as the transformer architecture (adopted in TransFusion and BEV-Fusion) suffers from limited paired RGB-LiDAR training data in the long tail. For transformers to work well in practice, they should be trained on diverse, large-scale datasets [11, 33, 47]. Further, end-to-end trained multi-modal detectors require paired multi-modal data for training. Therefore, we opt to study late-fusion of uni-modal detectors, which does not require paired RGB-LiDAR training data. CLOCs [41] is a late-fusion method that learns a standalone fusion network to merge RGB and LiDAR detections, showing promising results for 3D detection. More recently, [42] introduces a simple non-learned filtering algorithm that effectively removes false-positive LiDAR-detections that are far away from any 3D RGB detections. We delve into this simple (non-learned) late-fusion framework, study three crucial design choices, and present a method that significantly outperforms prior state-of-the-art methods for LT3D.

Long-Tailed Detection is not unique to the AV domain and has been well studied in 2D [18]. Existing methods propose reweighting losses [4, 9, 23, 29, 70], rebalancing data sampling [6, 12, 20, 74], balancing gradients computed from imbalanced classes [53], and balancing network weights [1]. CBGS [74] explicitly addresses rare-class 3D detection by up-sampling LiDAR sweeps with instances of rare classes, and pasting rare objects copied from different scenes. Although it works well for improving the detection accuracy of some classes (e.g., 5K~50K instances per

class), it does not significantly improve accuracy for rare classes (e.g., <5K instances per class). More recently, [31] adopts data augmentation via sampling, and [26] uses active learning and hard example mining to obtain more data for rare classes. LT3D presents distinct opportunities and challenges compared to 2D long-tailed detection because LiDAR sensors offer direct geometric and ego-motion cues that are difficult to extract from 2D images. Unlike 2D detectors, which must identify objects of various scales due to perspective image projection, 3D detectors do not experience as much scale variation for objects. However, LiDAR returns for far-field objects are sparse [19, 43], posing a different set of challenges. Additionally, rare classes, such as *child* and *stroller*, are typically small in size and have a limited number of LiDAR returns. As a result, LiDAR detectors struggle to accurately detect these rare classes. Our work addresses these issues by fusing RGB and LiDAR uni-modal detections.

3. Late-Fusion of RGB and LiDAR Detections

As depicted in Fig. 1, our simple late-fusion framework ensembles uni-modal 2D RGB and 3D LiDAR detectors. We first analyze different ways of incorporating RGB information in Sec. 3.1, present simple algorithms for matching RGB and LiDAR detections in Sec. 3.2, and finally describe score calibration, probabilistic fusion and NMS overlap fusion in Sec. 3.3.

3.1. How Do We Incorporate RGB Information?

Although LiDAR offers accurate localization, LiDAR-only detectors struggle to distinguish foreground objects from background using sparse LiDAR alone. RGB images provide complementary information that is essential for identifying objects and disambiguating those that are geometrically similar in point clouds but semantically different in images. Although prior works address late-fusion, they combine *3D RGB detectors* with 3D LiDAR detections [42]. In contrast, we find that *ensembling 2D RGB detectors* with 3D LiDAR detectors yields significantly better LT3D performance. We present insights on why using 2D detectors to incorporate RGB information yields better performance on rare categories below, and ablate the impact of using 2D versus 3D RGB detectors for late-fusion in Table 2.

2D RGB Detectors Are More Mature. 2D object detection is a fundamental problem in computer vision [13, 36, 50] that has matured in recent years and model trade-offs are well understood [37, 38, 48, 50]. In this work, we consider two state-of-the-art 2D RGB detectors, YOLOV7 [56] and DINO [68]. YOLOV7 is a real-time detector that identifies a number of training tricks that nearly doubles the inference efficiency over prior work without sacrificing performance. DINO is a recent transformer-based detector that improves upon DETR [5] using denoising anchor boxes. As 2D detectors do not make 3D predictions (e.g., depth and rotation), understanding how to best leverage them in the context of long-tailed 3D detection is a key challenge. We address this in Section 3.2.

2D RGB Detectors Can Be Trained with More Diverse Data. Training 2D RGB detectors only requires *2D bounding box* annotations, which are significantly cheaper to collect than 3D cuboids used for training 3D RGB detectors [27, 57]. Since annotating 3D amodal cuboids is both expensive and non-trivial (compared to bounding-box annotations for 2D detection), datasets for monocular 3D RGB detection are considerably smaller and less diverse than their 2D detection counterparts. For example, nuScenes [3] (published in 2020) annotates 144K RGB images of 23 classes, while COCO [36] (an early 2D detection dataset published in 2014) annotates 330K images of 80 classes. This allows us to pretrain 2D RGB detectors on significantly larger, more diverse, publicly available datasets [32, 49, 58, 63, 73]. We demonstrate that leveraging existing 2D detection datasets helps train stronger 2D detectors for “free”, further improving LT3D performance.

3.2. How Do We Match Uni-Modal Detections?

Finding correspondence between two sets of uni-modal detections is an essential step in the late-fusion framework (cf. Fig. 2B). Prior work [42] matches 3D RGB and 3D LiDAR detections using center distance in the bird’s-eye-

view (BEV) plane. However, precisely matching detections is difficult due to depth estimation errors from 3D RGB detectors. Instead, we opt to match *2D RGB* and 3D LiDAR detections. Prior work attempts to inflate 2D detections to the 3D BEV (using LiDAR points [59]), but we find that matching detections in the 3D BEV suffers from many of the same limitations as 3D RGB detections. Importantly, inflated 2D RGB detections impute additional depth estimation errors and reduce overall match quality. In contrast, we match multi-modal detections by projecting 3D LiDAR detections onto the 2D image plane, avoiding additional noise due to imprecise depth estimates. We ablate the impact of matching in the 3D BEV versus on the 2D image plane in Table 2, and present our 2D matching algorithm below.

Spatial Matching on the 2D Image Plane. Using the available sensor extrinsics, we project 3D LiDAR detections onto the 2D image plane. We then use the IoU metric to determine overlap between (projected) LiDAR and 2D RGB detections. A 2D RGB detection and a (projected) 3D LiDAR detection match if their IoU is greater than a fixed threshold. Although conceptually simple, we find that it works better than using center distance to match detections in the 3D BEV (cf. Table 2).

Handling Unmatched Detections. Spatially matching multi-modal detections using 2D IoU yields three categories of detections: matched detections, unmatched RGB detections (that do not have corresponding LiDAR detections), and unmatched LiDAR detections (that do not have corresponding RGB detections). We discuss how to fuse matched detections in the next subsection. For unmatched 2D RGB detections, we simply remove them. We posit that any unmatched RGB detections are likely to be false positives given that LiDAR detectors tend to yield high recall. On the other hand, we down-weight unmatched 3D LiDAR detections’ confidence scores by w . We set $w = 0.4$ in our work with a validation set.

Addressing Semantic Disagreement Between Modalities. As illustrated by Fig. 2C, detections may match spatially but not semantically. To address this, we propose a semantic matching heuristic to better fuse LiDAR and RGB detections. Given a pair of spatially matched RGB and LiDAR detections, we consider two cases. If both modalities predict the same semantic class, we perform score-fusion (described next). Otherwise, if both modalities predict different semantic classes, we use the confidence score and class label of the RGB-based detection. Intuitively, RGB detectors can predict semantics more reliably from high resolution images than LiDAR-only detectors. This helps correct misclassifications of geometrically similar, but semantically different objects produced by the 3D LiDAR detector, as shown in Fig. 3.

3.3. How Do We Fuse Matched Detections?

We combine matched detections with the same semantic class produced by different uni-modal detectors using probabilistic ensembling. However, the confidence scores of predictions from two detectors are not directly comparable. Therefore, we explore score calibration of RGB (x_{RGB}) and LiDAR (x_{LiDAR}) detections. Score calibration is crucial to fairly compare scores for fusion.

Score Calibration. Score fusion requires the scores from independent uni-modal detectors to be comparable. In this work, we tune a temperature τ_c for the logit score of class c before applying a sigmoid transform [7, 17], i.e., $\text{sigmoid}(\text{logit}_c/\tau_c)$. Optimally tuning per-class τ_c is computationally expensive. Therefore, we greedily tune each τ_c , optimizing per-class AP for each class progressively ordered by their cardinality.

Probabilistic Ensembling. Following [7], we assume independent class prior $p(c)$, and conditional independence given the class label c , i.e., $p(x_{\text{RGB}}, x_{\text{LiDAR}}|c) = p(x_{\text{RGB}}|c)p(x_{\text{LiDAR}}|c)$. We compute the final score as

$$\begin{aligned} & p(c|x_{\text{RGB}}, x_{\text{LiDAR}}) \\ = & p(x_{\text{RGB}}, x_{\text{LiDAR}}|c)p(c) / p(x_{\text{RGB}}, x_{\text{LiDAR}}) \\ \propto & p(x_{\text{RGB}}, x_{\text{LiDAR}}|c)p(c) \\ \propto & p(x_{\text{RGB}}|c)p(x_{\text{LiDAR}}|c)p(c) \\ \propto & p(c|x_{\text{RGB}})p(c|x_{\text{LiDAR}}) / p(c) \end{aligned}$$

where $p(c|x_{\text{RGB}})$ and $p(c|x_{\text{LiDAR}})$ are the posteriors after calibration. In the long-tailed scenario, $p(c)$ can significantly impact the final LT3D performance. To maximize performance, we need to jointly tune all class priors $p(c)$, which is computationally expensive in practice. Instead, we tune them greedily, one by one ordered by class cardinality.

NMS Overlapping Fusion. Neighboring cameras capture overlapping regions (Fig. 1-left), so some objects are detected and fused twice. After calibration, we simply run NMS in the overlapping regions [57] to remove lower-scoring detections.

4. Experiments

In this section, we conduct extensive experiments to evaluate our proposed approach. We compare our late-fusion approach with prior work and present a detailed ablation study that further addresses the three motivating questions in Fig. 2. We find that our proposed approach improves over prior works by 5.9% averaged over all classes, notably improving by 7.2% on rare classes (Table 1). We include benchmarking results on the Argoverse 2 dataset [60] in the supplement and find that the same conclusions hold.

Table 1. **Benchmarking on the nuScenes LT3D dataset.** Recall that our approach fuses 3D LiDAR and 2D RGB detections on the 2D image plane with score calibration and probabilistic ensembling. It performs the best on *all* categories, notably better than the end-to-end multi-modal BEVFusion [39] for classes with *medium* examples per class by 7.4% and *few* examples per class by 7.2%. We denote the modalities used in each method: C for RGB camera and L for LiDAR.

Method	Modality	All	Many	Medium	Few
FCOS3D [57]	C	20.9	39.0	23.3	2.9
BEVFormer[34]	C	27.3	52.3	31.6	1.4
PolarFormer [27]	C	28.0	54.0	31.6	2.2
CenterPoint [66]	L	39.2	76.4	43.1	3.5
TransFusion-L [2]	L	38.5	68.5	42.8	8.4
BEVFusion-L [39]	L	42.5	72.5	48.0	10.6
CMT-L [64]	L	34.7	73.4	35.9	1.1
CenterPoint [66] + RCNN [15]	C+L	34.0	64.8	37.5	4.3
TransFusion [2]	C+L	39.8	73.9	41.2	9.8
BEVFusion [39]	C+L	45.5	75.5	52.0	12.8
DeepInteraction [65]	C+L	43.7	76.2	51.1	7.9
CMT [64]	C+L	44.4	79.9	53.0	4.8
CenterPoint + FCOS3D [42]	C+L	43.6	77.1	49.0	9.4
Ours	C+L	51.4	77.9	59.4	20.0

4.1. Experiment Setup

Datasets. We study LT3D using the well-established nuScenes dataset [3]. We follow the protocol defined by [42], using all 18 long-tail categories (with sufficient examples in the validation set). Moreover, we use the nuImages dataset [3] as an external 2D annotated data source to study how using additional data to train better 2D RGB detectors improves late-fusion performance. Lastly, we evaluate our approach on Argoverse 2 in the supplement and find that our primary conclusions hold. Note that other datasets such as KITTI [14] and Waymo [52] do not support the study of LT3D because they only annotate three common classes.

Metrics. Mean average precision (mAP) is an established metric for object detection [36]. For 3D detection, a true positive (TP) is defined as a detection that has a center distance within a distance threshold on the ground-plane to a ground-truth annotation [3]. mAP computes the mean of AP over all classes, where per-class AP is the area under the precision-recall curve drawn with distance thresholds of [0.5, 1, 2, 4] meters. We report the metrics for three groups of classes based on their cardinality: *Many* (>50k training instances per class), *Medium* (5k~50k), and *Few* (<5k). Following [42], we use the official nuScenes train-set for training and report numbers on the val-set.

Implementation Details. We retrain several existing LiDAR-only, RGB-only, and multi-modal detectors on all 18 classes in the nuScenes LT3D setup. We employ standard augmentation techniques, including copy-paste augmentation and adopt the sampling ratios defined by [42] when training all detectors. Following established practices, we aggregate the past 10 sweeps for LiDAR densification

Table 2. **Fusing Uni-modal Detections in the 3D BEV vs. on the 2D Image Plane.** We evaluate the impact of fusing 3D LiDAR detections (from CenterPoint trained with hierarchical loss [42]) with 2D RGB and 3D RGB detections in both the 3D BEV and 2D image plane. We match and filter detections in the 3D BEV using center distance as proposed by [42], and match and filter detections in the 2D image plane using IoU. Following [59], we inflate 2D detections to the 3D BEV using LiDAR points within the box frustum. We project 3D detections to the 2D plane using provided sensor extrinsics. We find that matching 3D RGB detections in the 3D BEV and in the 2D image plane yields similar results. Unsurprisingly, inflating 2D RGB detections for matching in the 3D BEV performs worse than matching 3D RGB detections in the 3D BEV. In contrast, filtering LiDAR-based detections using 2D detections in the 2D image plane (bottom right panel) significantly improves performance for classes with medium and few examples by >10 mAP. This suggests that 2D detectors achieve better detection performance compared to 3D RGB detectors. We further verify this in Table 3.

Method	Fusion in 3D BEV				Fusion on 2D Image Plane			
	All	Many	Medium	Few	All	Many	Medium	Few
CenterPoint	40.4	77.1	45.1	4.3	40.4	77.1	45.1	4.3
+ FCOS3D [57]	42.9	76.6	48.7	8.1	42.6	75.0	49.4	7.7
+ BEVFormer [34]	43.2	76.9	50.8	6.3	42.8	75.2	51.4	5.7
+ PolarFormer [27]	42.8	76.8	50.0	6.1	42.6	75.1	51.1	5.6
+ YOLOV7 [56]	40.1	76.1	43.8	5.8	45.7	77.1	52.8	11.2
+ DINO [68]	40.3	76.2	44.1	5.9	49.5	77.4	57.7	16.7

using the provided ego-vehicle poses.

We use the open-source implementations from [42] for training FCOS3D, CenterPoint, and TransFusion, and the first-party implementations for other detectors, following the training schedule proposed by each respective paper. We train our model with 8 RTX 3090 GPUs. By default, we train the 2D RGB detector with 2D bounding boxes derived from nuScenes’ 3D annotations and additionally train with 2D bounding boxes from nuImages where denoted. Our 2D RGB detectors, YOLOV7 and DINO, are pre-trained on the ImageNet [10] and COCO [36] datasets.

4.2. Comparison to the State-of-the-Art

We compare our late-fusion approach against prior work in Table 1, and present qualitative results in Fig. 3. We adapt existing methods (which were previously trained on the standard 10 class in the official nuScenes benchmark) for LT3D by retraining them on all 18 classes.

CenterPoint [66], a popular 3D LiDAR detector, is unable to detect rare objects, achieving just 3.5% AP on classes with f_{ew} examples. This is expected as it is difficult to identify rare objects from sparse LiDAR points alone. Perhaps surprisingly, the transformer-based 3D LiDAR detector BEVFusion-L performs considerably better on rare classes, achieving 10.6% AP. However, BEVFusion-L performs 3.9% worse than CenterPoint on common classes. We posit that limited training data in-the-tail and class imbalance makes it difficult to learn robust features.

Table 3. **Evaluating 2D Detection Performance.** We find that simply projecting 3D detections from RGB-only detectors to 2D yields considerably lower 2D detection accuracy across all classes. However, 2D RGB detectors achieve higher performance. Intuitively, 2D RGB detectors achieve better classification performance and predict tighter fitting bounding boxes than those derived by projecting 3D detections to the image plane. This explains why fusing detections from 2D RGB detectors yields better LT3D performance than detections from 3D RGB detectors. All detectors in this table are only trained on the nuScenes train-set.

Method	All	Many	Medium	Few
FCOS3D (3D RGB Detector)	18.3	36.0	21.1	0.2
BEVFormer (3D RGB Detector)	23.0	40.8	28.2	2.1
PolarFormer (3D RGB Detector)	20.7	37.5	25.2	1.6
YOLOV7 (2D RGB Detector)	37.5	63.5	45.0	7.1
DINO (2D RGB Detector)	44.3	67.8	51.9	15.9

In contrast, BEVFusion [34], which is an end-to-end trained multi-modal method, performs better than the LiDAR-only variant (BEVFusion-L), confirming the benefit of using multi-modal input for LT3D. Next, we implement a simple baseline that trains a region-based CNN (RCNN) [15] classifier on cropped regions corresponding to projected 3D detections. It underperforms CenterPoint, presumably because learning classifiers on cropped regions does not exploit contextual information and leads to worse classification accuracy. Peri et. al. [42] introduces a simple filtering algorithm that keeps CenterPoint detections that are close (based on center distance) to monocular 3D RGB detections produced by FCOS3D in the BEV, and discards all other LiDAR predictions. Given the success of this simple approach, we study this late-fusion paradigm further. By carefully considering design choices outlined in Fig. 2, we improve over [42] by 7.8%.

4.3. Ablation Study

In this section, we design a set of experiments to study the trade-off between using 2D and 3D RGB detectors, and matching in the 2D image and 3D BEV plane (cf. Table 2). Further, we examine the impact of using additional data and study different fusion strategies (cf. Table 4). Our analysis confirms that 2D RGB detectors are better suited for late-fusion, matching projected 3D LiDAR detections in the 2D image-plane outperforms matching 3D RGB detections in the 3D BEV, and score calibration prior to probabilistic fusion improves performance.

How Do We Incorporate RGB Information? Although LiDAR-based detectors are widely adopted for 3D detection, they produce many high-scoring false positives (FPs) for rare classes due to misclassification. We focus on removing such FPs using an RGB-based detector by leveraging two insights: (1) LiDAR-based 3D detections are accurate w.r.t 3D localization and yield high recall (though classification is poor), and (2) RGB-based detections are accurate w.r.t recognition (though 3D localization is poor).



Figure 4. Both our method (columns 1-3) and TransFusion [2] (columns 4 -5) share the same failure cases. In the first and second row, the 2D RGB detector DINO detects the heavily occluded cars but 3D LiDAR detector fails to detect them. As a result, the late-fusion predictions miss these cars because our method throws away unmatched RGB detections since we do not have accurate 3D information. In the third row, we see that although both the LiDAR and RGB detectors fire on the object (whose ground-truth label is `police-officer`), the LiDAR detector classifies it as `adult` and RGB detector classifies it as `construction-worker`. As a result, the final detection is incorrect w.r.t the predicted categorical label. TransFusion also misclassifies this object as an `adult`.

Table 4. **Ablation on Late Fusion.** Our analysis confirms that 2D RGB detectors are better suited for late-fusion, matching projected 3D LiDAR detections on the 2D image-plane outperforms matching 2D RGB detections inflated to the 3D BEV, and score calibration prior to NMS overlap fusion and probabilistic fusion improves performance.

Method	All	Many	Medium	Few
CenterPoint w/ Hierarchy [42]	40.4	77.1	45.1	4.3
+ 2D Img. Filtering w/ DINO	47.9	77.1	55.8	14.4
+ External Data	49.8	77.1	57.1	18.6
+ Score Calibration	50.5	77.8	58.2	18.7
+ NMS Overlap Fusion	50.9	77.9	59.2	18.7
+ Probabilistic Ensembling	51.4	77.9	59.4	20.0

We incorporate RGB information by matching and filtering 3D LiDAR detections with RGB-based detections. We evaluate the impact of using 2D RGB-based detectors (e.g., YOLOV7 and DINO) versus 3D RGB-based detectors (e.g., FCOS3D, BEVFormer, PolarFormer) in Table 2.

In this work, we consider the impact of matching LiDAR detections with 3D RGB detections in the 3D BEV and 2D image plane. Similarly, we consider the impact of matching LiDAR detections with 2D RGB detections in the 3D BEV and 2D image plane. Importantly, we find that matching LiDAR detections with 2D RGB detections in the 2D image plane significantly improves performance.

How Do We Match Detections From Uni-Modal Detectors? To match 3D detections on the 2D image plane, we use the provided sensor extrinsics. To match 2D detections in the 3D BEV, we inflate 2D detection using LiDAR points within the box frustum. In practice, we find that naively lifting 2D RGB detections into 3D leads to imprecise depth estimates and lower performance.

To match and filter LiDAR and RGB detections in the 3D BEV, we follow the procedure prescribed by [42]. For each RGB-based detection, we keep LiDAR-based detections within a radius of m meters and remove all the others that are not close to any RGB-based detections. This works well for 3D RGB detections. Late fusion with FCOS3D, BEVFormer, and PolarFormer improves over the LiDAR-only model by 2% averaged over all classes (cf. Table 2). Unsurprisingly, we find that matching inflated 2D RGB detections in the 3D BEV performs worse than matching 3D RGB detections in the 3D BEV, notably achieving lower accuracy than the LiDAR-only baseline. To match and filter LiDAR and RGB detections on the 2D image plane, we simply use the IoU metric. Two detections are considered matched if their spatial overlap exceeds a fixed threshold. We find that projecting LiDAR detections on the 2D image plane and fusing them using 2D RGB detections significantly improves performance for classes with `medium` and `few` examples by more than 10%. In contrast, we find that projecting 3D RGB detections for matching on the 2D image plane performs worse than matching 2D RGB detections on the 2D image plane, suggesting that 2D detectors achieve better recognition performance than 3D RGB detectors. Table 3 shows that 2D detectors (e.g., DINO) outperform state-of-the-art 3D RGB detectors (e.g., BEVFormer) for 2D detection on the nuScenes val-set. Importantly, DINO performs significantly better than BEVFormer (15.9 vs. 2.1 mAP) on rare classes.

How Do We Fuse Matched Detections? Prior to fusion, we first calibrate the scores of LiDAR and RGB detections to ensure that they are comparable. This improves accuracy by 0.7% averaged over all classes, notably improving performance for classes with a `medium` number of exam-

Table 5. **Per-class Performance on nuScenes.** Our late-fusion approach achieves the highest per-class AP on 6 out of 10 classes. Compared to DeepInteraction, our approach improves construction worker by 15.2 %, stroller by 6.8 %, and pushable-pullable by 17.3 %. Note, CV is construction vehicle, MC is motorcycle, PP is pushable-pullable, CW is construction-worker, and Stro. is stroller. We highlight classes with Medium and Few examples per class in blue.

Method	Car	Adult	Truck	CV	Bicy	MC	Child	CW	Stro.	PP
TransFusion [2]	84.4	84.2	58.4	24.5	46.7	60.8	3.1	21.6	13.3	25.3
BEVFusion [39]	90.2	67.2	65.5	35.2	58.8	77.0	4.4	39.0	29.6	34.1
DeepInteraction [65]	84.9	85.9	63.2	35.3	64.3	76.2	6.0	30.7	30.9	30.8
CMT [64]	88.6	87.7	65.2	36.9	66.7	76.3	4.7	34.4	9.4	34.1
CP + FCOS3D [42]	88.5	86.6	63.4	29.0	58.5	68.2	5.3	35.8	31.6	39.3
Ours	86.3	86.2	60.6	35.3	70.1	75.9	8.8	55.9	37.7	58.1

ples. To remove duplicate detections in overlapping regions between neighboring cameras, we use NMS overlap fusion to further improve accuracy by 0.4 mAP across all classes. When using probabilistic ensembling, we use Bayesian fusion to reason about the final score of matched detections. Concretely, if two matched detections fire in the same place, the fused score should be higher than the individual scores because there is twice the evidence of an object at that particular spatial location. As shown in Table 4, probabilistic ensembling further improves accuracy by 0.5 mAP.

Per-Class Breakdown Results. We highlight the per-class performance of recent multi-modal methods in Table 5. All multi-modal methods perform similarly on common classes. However, we find that all multi-modal methods perform considerably worse on classes in-the-tail compared to common classes, highlighting the need for further investigation by the research community. Notably, our late-fusion approach achieves 20% higher AP on pushable-pullable and 6% higher AP on stroller than prior work. In general, our late-fusion approach yields considerable improvement on classes with medium and few examples. Despite significant improvements in rare class detection accuracy, our approach detects child with 8% AP. We posit that it is difficult to differentiate child from adult due to perspective geometry, since a small child close to the camera looks similar to a tall adult far away from the camera.

Failure Cases and Visualizations. We visualize common failure cases of our late-fusion approach and compare them with the failure cases of TransFusion, an end-to-end trained multi-modal detector. We find that our method fails in cases of occlusions (where there is no 3D information) and in cases where the 2D RGB detector misclassifies the object. See Fig. 4 for detailed analysis.

4.4. Limitations and Future Work

Our work focuses on LT3D, a problem that emphasizes 3D object detection for rare classes which are often safety-

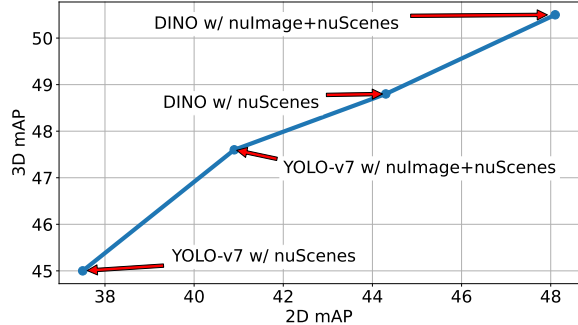


Figure 5. Although nuScenes is a 3D detection benchmark, we can generate 2D annotations using the provided sensor extrinsics by projecting the 3D annotations to the 2D image plane. We find that evaluating 2D detectors using these 2D nuScenes annotations is a good proxy task (x-axis) that is positively correlated with the downstream performance of the full late-fusion pipeline (y-axis). Concretely, training 2D detectors with more data (e.g., training with nuScenes and nulgages), and using better 2D detectors (e.g., DINO) improves performance on the proxy task as well as the downstream late-fusion algorithm.

critical for AVs, like stroller and debris. Therefore, improving LT3D is important for ensuring safe autonomy. However, our work does not directly study how addressing LT3D affects downstream perception tasks. Future work should address this limitation. While our late-fusion pipeline can fuse detections from any detectors, we focus on fusing only detections from uni-modal detectors. We hope future work will study fusing detections from more uni- and multi-modal detectors.

Moreover, as shown in Fig. 5, simply training better 2D RGB detectors with more data provides a natural pathway for improving LT3D performance. We find that 2D detection accuracy on nuScenes is a strong proxy for final 3D LT3D performance. Recent works in large-scale vision language models [40, 69, 71] show promising zero-shot results in detecting rare classes. Identifying ways of incorporating foundation models into our late-fusion framework can greatly improve LT3D.

5. Conclusion

We present a detailed exploration of late-fusion, focused on addressing three key design decisions. We find that 2D RGB detectors are better suited for late-fusion, matching projected 3D LiDAR detections on the 2D image-plane outperforms matching 2D RGB detections inflated to the 3D BEV, and score calibration prior to NMS overlap fusion and probabilistic fusion improves performance. Our simple late-fusion approach achieves state-of-the-art performance, improving over prior work by 5.9% mAP. Despite the success of transformers in other computer vision and natural language domains, we find that end-to-end transformer-based multi-modal detectors still struggle to detect rare classes.

References

- [1] Shaden Alshammari, Yu-Xiong Wang, Deva Ramanan, and Shu Kong. Long-tailed recognition via weight balancing. In *CVPR*, 2022. 3
- [2] Xuyang Bai, Zeyu Hu, Xinge Zhu, Qingqiu Huang, Yilun Chen, Hongbo Fu, and Chiew-Lan Tai. Transfusion: Robust lidar-camera fusion for 3d object detection with transformers. In *CVPR*, 2022. 2, 5, 7, 8, 12
- [3] Holger Caesar, Varun Bankiti, Alex H Lang, Sourabh Vora, Venice Erin Liong, Qiang Xu, Anush Krishnan, Yu Pan, Giancarlo Baldan, and Oscar Beijbom. nuscenes: A multimodal dataset for autonomous driving. In *Proceedings of the CVPR, 2020*. 1, 4, 5
- [4] Kaidi Cao, Colin Wei, Adrien Gaidon, Nikos Arechiga, and Tengyu Ma. Learning imbalanced datasets with label-distribution-aware margin loss. In *NeurIPS*, 2019. 3
- [5] Nicolas Carion, Francisco Massa, Gabriel Synnaeve, Nicolas Usunier, Alexander Kirillov, and Sergey Zagoruyko. End-to-end object detection with transformers. In *ECCV*, 2020. 2, 4
- [6] Nitesh V Chawla, Kevin W Bowyer, Lawrence O Hall, and W Philip Kegelmeyer. Smote: synthetic minority over-sampling technique. *Journal of Artificial Intelligence Research*, 16:321–357, 2002. 3
- [7] Yi-Ting Chen, Jinghao Shi, Zelin Ye, Christoph Mertz, Deva Ramanan, and Shu Kong. Multimodal object detection via probabilistic ensembling. In *ECCV*, 2022. 5
- [8] Hsu-kuang Chiu, Antonio Prioletti, Jie Li, and Jeanette Bohg. Probabilistic 3d multi-object tracking for autonomous driving. *CoRR*, abs/2001.05673, 2020. 2
- [9] Yin Cui, Menglin Jia, Tsung-Yi Lin, Yang Song, and Serge Belongie. Class-balanced loss based on effective number of samples. In *CVPR*, 2019. 3
- [10] Jia Deng, Wei Dong, Richard Socher, Li-Jia Li, Kai Li, and Li Fei-Fei. Imagenet: A large-scale hierarchical image database. In *CVPR*, 2009. 6
- [11] Alexey Dosovitskiy, Lucas Beyer, Alexander Kolesnikov, Dirk Weissenborn, Xiaohua Zhai, Thomas Unterthiner, Mostafa Dehghani, Matthias Minderer, Georg Heigold, Sylvain Gelly, et al. An image is worth 16x16 words: Transformers for image recognition at scale. *arXiv:2010.11929*, 2020. 3
- [12] Chris Drummond, Robert C Holte, et al. C4. 5, class imbalance, and cost sensitivity: why under-sampling beats over-sampling. In *Workshop on learning from imbalanced datasets II*, 2003. 3
- [13] Pedro F Felzenszwalb, Ross B Girshick, David McAllester, and Deva Ramanan. Object detection with discriminatively trained part-based models. *IEEE transactions on pattern analysis and machine intelligence*, 32(9):1627–1645, 2009. 4
- [14] Andreas Geiger, Philip Lenz, and Raquel Urtasun. Are we ready for autonomous driving? the kitti vision benchmark suite. In *CVPR*, 2012. 1, 5
- [15] Ross Girshick, Jeff Donahue, Trevor Darrell, and Jitendra Malik. Region-based convolutional networks for accurate object detection and segmentation. *IEEE transactions on pattern analysis and machine intelligence*, 38(1):142–158, 2015. 5, 6
- [16] Vitor Guizilini, Rares Ambrus, Sudeep Pillai, Allan Raventos, and Adrien Gaidon. 3d packing for self-supervised monocular depth estimation. In *CVPR*, 2020. 2
- [17] Chuan Guo, Geoff Pleiss, Yu Sun, and Kilian Q Weinberger. On calibration of modern neural networks. In *ICML*, 2017. 5
- [18] Agrim Gupta, Piotr Dollar, and Ross Girshick. Lvis: A dataset for large vocabulary instance segmentation. In *CVPR*, 2019. 3
- [19] Shubham Gupta, Jeet Kanjani, Mengtian Li, Francesco Ferroni, James Hays, Deva Ramanan, and Shu Kong. Far3det: Towards far-field 3d detection. In *Proceedings of the IEEE/CVF Winter Conference on Applications of Computer Vision*, 2023. 2, 3
- [20] Hui Han, Wen-Yuan Wang, and Bing-Huan Mao. Borderline-smote: a new over-sampling method in imbalanced data sets learning. In *International Conference on Intelligent Computing*, 2005. 3
- [21] Qingdong He, Zhengning Wang, Hao Zeng, Yi Zeng, Yijun Liu, Shuaicheng Liu, and Bing Zeng. Stereo rgb and deeper lidar-based network for 3d object detection in autonomous driving. *IEEE Transactions on Intelligent Transportation Systems*, 24(1):152–162, 2022. 2
- [22] Yihan Hu, Jiazhi Yang, Li Chen, Keyu Li, Chonghao Sima, Xizhou Zhu, Siqi Chai, Senyao Du, Tianwei Lin, Wenhai Wang, Lewei Lu, Xiaosong Jia, Qiang Liu, Jifeng Dai, Yu Qiao, and Hongyang Li. Planning-oriented autonomous driving. In *CVPR*, 2023. 2
- [23] Chen Huang, Yining Li, Chen Change Loy, and Xiaoou Tang. Deep imbalanced learning for face recognition and attribute prediction. *PAMI*, 42(11):2781–2794, 2019. 3
- [24] Junjie Huang and Guan Huang. Bevdet4d: Exploit temporal cues in multi-camera 3d object detection. *arXiv:2203.17054*, 2022. 2
- [25] Junjie Huang, Guan Huang, Zheng Zhu, and Dalong Du. Bevdet: High-performance multi-camera 3d object detection in bird-eye-view. *arXiv:2112.11790*, 2021. 2
- [26] Chiyu Max Jiang, Mahyar Najibi, Charles R Qi, Yin Zhou, and Dragomir Anguelov. Improving the intra-class long-tail in 3d detection via rare example mining. In *European Conference on Computer Vision*, pages 158–175. Springer, 2022. 3

- [27] Yanqin Jiang, Li Zhang, Zhenwei Miao, Xiatian Zhu, Jin Gao, Weiming Hu, and Yu-Gang Jiang. Polarformer: Multi-camera 3d object detection with polar transformers. *arXiv:2206.15398*, 2022. 2, 4, 5, 6
- [28] Yang Jiao, Zequn Jie, Shaoxiang Chen, Jingjing Chen, Xiaolin Wei, Lin Ma, and Yu-Gang Jiang. Msmdfusion: Fusing lidar and camera at multiple scales with multi-depth seeds for 3d object detection. *arXiv:2209.03102*, 2022. 2
- [29] Salman H Khan, Munawar Hayat, Mohammed Benamoun, Ferdous A Sohel, and Roberto Togneri. Cost-sensitive learning of deep feature representations from imbalanced data. *IEEE transactions on neural networks and learning systems*, 29(8):3573–3587, 2017. 3
- [30] Alex H. Lang, Sourabh Vora, Holger Caesar, Lubing Zhou, Jiong Yang, and Oscar Beijbom. Pointpillars: Fast encoders for object detection from point clouds. In *CVPR*, 2019. 2
- [31] Daeun Lee and Jinkyu Kim. Resolving class imbalance for lidar-based object detector by dynamic weight average and contextual ground truth sampling. In *Proceedings of the IEEE/CVF Winter Conference on Applications of Computer Vision*, pages 682–691, 2023. 3
- [32] Liunian Harold Li, Pengchuan Zhang, Haotian Zhang, Jianwei Yang, Chunyuan Li, Yiwu Zhong, Lijuan Wang, Lu Yuan, Lei Zhang, Jenq-Neng Hwang, et al. Grounded language-image pre-training. In *CVPR*, 2022. 4
- [33] Yingwei Li, Adams Wei Yu, Tianjian Meng, Ben Caine, Jiquan Ngiam, Daiyi Peng, Junyang Shen, Yifeng Lu, Denny Zhou, Quoc V Le, et al. Deepfusion: Lidar-camera deep fusion for multi-modal 3d object detection. In *CVPR*, 2022. 3
- [34] Zhiqi Li, Wenhai Wang, Hongyang Li, Enze Xie, Chonghao Sima, Tong Lu, Yu Qiao, and Jifeng Dai. Bevformer: Learning bird’s-eye-view representation from multi-camera images via spatiotemporal transformers. In *ECCV*, 2022. 2, 5, 6, 12
- [35] Ming Liang, Bin Yang, Yun Chen, Rui Hu, and Raquel Urtasun. Multi-task multi-sensor fusion for 3d object detection. In *Proceedings of the CVPR*, pages 7345–7353, 2019. 2
- [36] Tsung-Yi Lin, Michael Maire, Serge J. Belongie, James Hays, Pietro Perona, Deva Ramanan, Piotr Dollár, and C. Lawrence Zitnick. Microsoft COCO: common objects in context. In *ECCV*, 2014. 4, 5, 6
- [37] Tsung-Yi Lin, Priya Goyal, Ross Girshick, Kaiming He, and Piotr Dollár. Focal loss for dense object detection. In *ICCV*, 2017. 4
- [38] Wei Liu, Dragomir Anguelov, Dumitru Erhan, Christian Szegedy, Scott Reed, Cheng-Yang Fu, and Alexander C Berg. Ssd: Single shot multibox detector. In *ECCV*, 2016. 2, 4
- [39] Zhijian Liu, Haotian Tang, Alexander Amini, Xinyu Yang, Huizi Mao, Daniela Rus, and Song Han. Bev-fusion: Multi-task multi-sensor fusion with unified bird’s-eye view representation. *arXiv:2205.13542*, 2022. 1, 2, 5, 8, 12
- [40] Matthias Minderer, Alexey Gritsenko, and Neil Houlsby. Scaling open-vocabulary object detection. *arXiv:2306.09683*, 2023. 8
- [41] Su Pang, Daniel Morris, and Hayder Radha. Clocs: Camera-lidar object candidates fusion for 3d object detection. In *IEEE/RSJ International Conference on Intelligent Robots and Systems (IROS)*, 2020. 3
- [42] Neehar Peri, Achal Dave, Deva Ramanan, and Shu Kong. Towards long-tailed 3d detection. In *Conference on Robot Learning (CoRL)*, 2022. 1, 3, 4, 5, 6, 7, 8, 12
- [43] Neehar Peri, Mengtian Li, Benjamin Wilson, Yu-Xiong Wang, James Hays, and Deva Ramanan. An empirical analysis of range for 3d object detection. In *Proceedings of the IEEE/CVF International Conference on Computer Vision*, pages 4074–4083, 2023. 3, 12
- [44] Jonah Philion and Sanja Fidler. Lift, splat, shoot: Encoding images from arbitrary camera rigs by implicitly unprojecting to 3d. In *ECCV*, 2020. 2
- [45] Charles R Qi, Wei Liu, Chenxia Wu, Hao Su, and Leonidas J Guibas. Frustum pointnets for 3d object detection from rgb-d data. In *IEEE conference on computer vision and pattern recognition*, 2018. 2
- [46] Charles R Qi, Hao Su, Kaichun Mo, and Leonidas J Guibas. Pointnet: Deep learning on point sets for 3d classification and segmentation. In *Proceedings of the IEEE conference on computer vision and pattern recognition*, pages 652–660, 2017. 2
- [47] Alec Radford, Jong Wook Kim, Chris Hallacy, Aditya Ramesh, Gabriel Goh, Sandhini Agarwal, Girish Sastry, Amanda Askell, Pamela Mishkin, Jack Clark, et al. Learning transferable visual models from natural language supervision. In *International conference on machine learning*, pages 8748–8763. PMLR, 2021. 3
- [48] Joseph Redmon, Santosh Divvala, Ross Girshick, and Ali Farhadi. You only look once: Unified, real-time object detection. In *Proceedings of the IEEE conference on computer vision and pattern recognition*, pages 779–788, 2016. 4
- [49] Joseph Redmon and Ali Farhadi. Yolo9000: better, faster, stronger. In *Proceedings of the IEEE conference on computer vision and pattern recognition*, pages 7263–7271, 2017. 4
- [50] Shaoqing Ren, Kaiming He, Ross Girshick, and Jian Sun. Faster r-cnn: Towards real-time object detection with region proposal networks. In *Advances in Neural Information Processing Systems*, 2015. 4

- [51] Shaoshuai Shi, Li Jiang, Jiajun Deng, Zhe Wang, Chaoxu Guo, Jianping Shi, Xiaogang Wang, and Hongsheng Li. Pv-rcnn++: Point-voxel feature set abstraction with local vector representation for 3d object detection. *International Journal of Computer Vision*, pages 1–21, 2022. 2
- [52] Pei Sun, Henrik Kretzschmar, Xerxes Dotiwalla, Aurelien Chouard, Vijaysai Patnaik, Paul Tsui, James Guo, Yin Zhou, Yuning Chai, Benjamin Caine, Vijay Vasudevan, Wei Han, Jiquan Ngiam, Hang Zhao, Aleksei Timofeev, Scott Ettinger, Maxim Krivokon, Amy Gao, Aditya Joshi, Yu Zhang, Jonathon Shlens, Zhifeng Chen, and Dragomir Anguelov. Scalability in perception for autonomous driving: Waymo open dataset. In *CVPR (CVPR)*, 2020. 1, 5
- [53] Kaihua Tang, Jianqiang Huang, and Hanwang Zhang. Long-tailed classification by keeping the good and removing the bad momentum causal effect. In *NeurIPS*, 2020. 3
- [54] Zhi Tian, Chunhua Shen, Hao Chen, and Tong He. Fcos: Fully convolutional one-stage object detection. In *Proceedings of the IEEE/CVF international conference on computer vision*, pages 9627–9636, 2019. 2
- [55] Sourabh Vora, Alex H Lang, Bassam Helou, and Oscar Beijbom. Pointpainting: Sequential fusion for 3d object detection. In *CVPR*, 2020. 2
- [56] Chien-Yao Wang, Alexey Bochkovskiy, and Hong-Yuan Mark Liao. Yolov7: Trainable bag-of-freebies sets new state-of-the-art for real-time object detectors. *arXiv:2207.02696*, 2022. 4, 6
- [57] Tai Wang, Xinge Zhu, Jiangmiao Pang, and Dahua Lin. FCOS3D: fully convolutional one-stage monocular 3d object detection. In *ICCV*, 2021. 1, 2, 4, 5, 6, 12
- [58] Xudong Wang, Zhaowei Cai, Dashan Gao, and Nuno Vasconcelos. Towards universal object detection by domain attention. In *Proceedings of the CVPR*, pages 7289–7298, 2019. 4
- [59] Benjamin Wilson, Zsolt Kira, and James Hays. 3d for free: Crossmodal transfer learning using hd maps. *arXiv:2008.10592*, 2020. 2, 4, 6
- [60] Benjamin Wilson, William Qi, Tanmay Agarwal, John Lambert, Jagjeet Singh, Siddhesh Khandelwal, Bowen Pan, Ratnesh Kumar, Andrew Hartnett, Jhony Kaesemodel Pontes, et al. Argoverse 2: Next generation datasets for self-driving perception and forecasting. *arXiv preprint arXiv:2301.00493*, 2023. 5
- [61] Benjamin Wilson, William Qi, Tanmay Agarwal, John Lambert, Jagjeet Singh, Siddhesh Khandelwal, Bowen Pan, Ratnesh Kumar, Andrew Hartnett, Jhony Kaesemodel Pontes, Deva Ramanan, Peter Carr, and James Hays. Argoverse 2: Next generation datasets for self-driving perception and forecasting. In *Neural Information Processing Systems Datasets and Benchmarks Track*, 2021. 1
- [62] Danfei Xu, Dragomir Anguelov, and Ashesh Jain. Pointfusion: Deep sensor fusion for 3d bounding box estimation. In *IEEE conference on computer vision and pattern recognition*, 2018. 2
- [63] Hang Xu, Linpu Fang, Xiaodan Liang, Wenxiong Kang, and Zhenguo Li. Universal-rcnn: Universal object detector via transferable graph r-cnn. In *AAAI*, 2020. 4
- [64] Junjie Yan, Yingfei Liu, Jianjian Sun, Fan Jia, Shuailin Li, Tiancai Wang, and Xiangyu Zhang. Cross modal transformer via coordinates encoding for 3d object detection. *arXiv:2301.01283*, 2023. 5, 8, 12
- [65] Zeyu Yang, Jiaqi Chen, Zhenwei Miao, Wei Li, Xiaotian Zhu, and Li Zhang. Deepinteraction: 3d object detection via modality interaction. In *NeurIPS*, 2022. 5, 8, 12
- [66] Tianwei Yin, Xingyi Zhou, and Philipp Krahenbuhl. Center-based 3d object detection and tracking. In *CVPR*, 2021. 1, 2, 5, 6, 12
- [67] Tianwei Yin, Xingyi Zhou, and Philipp Krähenbühl. Multimodal virtual point 3d detection. *NeurIPS*, 2021. 2
- [68] Hao Zhang, Feng Li, Shilong Liu, Lei Zhang, Hang Su, Jun Zhu, Lionel Ni, and Harry Shum. Dino: Detr with improved denoising anchor boxes for end-to-end object detection. In *International Conference on Learning Representations*, 2022. 4, 6
- [69] Haotian Zhang, Pengchuan Zhang, Xiaowei Hu, Yenchun Chen, Liunian Li, Xiyang Dai, Lijuan Wang, Lu Yuan, Jenq-Neng Hwang, and Jianfeng Gao. Glipv2: Unifying localization and vision-language understanding. *NeurIPS*, 2022. 8
- [70] Songyang Zhang, Zeming Li, Shipeng Yan, Xuming He, and Jian Sun. Distribution alignment: A unified framework for long-tail visual recognition. In *CVPR*, 2021. 3
- [71] Xingyi Zhou, Rohit Girdhar, Armand Joulin, Philipp Krähenbühl, and Ishan Misra. Detecting twenty-thousand classes using image-level supervision. In *European Conference on Computer Vision*, 2022. 8
- [72] Xingyi Zhou, Vladlen Koltun, and Philipp Krähenbühl. Tracking objects as points. *CoRR*, abs/2004.01177, 2020. 2
- [73] Xingyi Zhou, Vladlen Koltun, and Philipp Krähenbühl. Simple multi-dataset detection. In *CVPR*, 2022. 4
- [74] Benjin Zhu, Zhengkai Jiang, Xiangxin Zhou, Zeming Li, and Gang Yu. Class-balanced grouping and sampling for point cloud 3d object detection. *arXiv:1908.09492*, 2019. 2, 3

A. Transformer-Based LiDAR Detectors

In the main paper, we evaluate all late-fusion methods by filtering LiDAR detections from CenterPoint with different RGB detectors. However, our late-fusion approach generalizes to other 3D LiDAR detectors as well. To this end, we evaluate our best-performing late-fusion configuration from the main paper with LiDAR detections from BEVFusion-L [39] in Table 6.

First, we note that BEVFusion-L performs 2.1% better than CenterPoint on LT3D, notably improving on classes with few examples by 6.2%. However, BEVFusion-L performs 4.6% worse than CenterPoint on classes with many examples, suggesting that learning robust features for both common and rare categories is challenging. We find that filtering BEVFusion-L’s 3D detections with YOLOV7’s 2D detections in the image plane yields a 4.8% improvement overall, and a 7.8% improvement on rare classes. Replacing YOLOV7 with DINO’s 2D detections yields a further 2.4% improvement overall, and a 0.7% AP improvement for rare classes. This further supports our hypothesis that late-fusion with better 2D detectors can improve LT3D accuracy. In contrast, the end-to-end multi-modal variant of BEVFusion only improves over the LiDAR-only baseline by 3% overall, and performs 5.2% worse than our late-fusion approach.

Table 6. **Transformer-based 3D LiDAR Detector.** We evaluate the late-fusion performance of BEVFusion-L (LiDAR-only) with YOLOV7 and DINO, and find that our late fusion strategy (with DINO) improves over the LiDAR-only model by 8.2% overall and 8.5% AP for rare classes. This suggests that our late-fusion approach generalizes across different 3D detector architectures.

Method	All	Many	Medium	Few
CenterPoint w/ Hier. [42]	40.4	77.1	45.1	4.3
+ 2D Img. Filtering w/ YOLOV7	47.6	77.4	54.6	14.6
+ 2D Img. Filtering w/ DINO	51.4	77.9	59.4	20.0
BEVFusion-L	42.5	72.5	48.0	10.6
+ 2D Img. Filtering w/ YOLOV7	48.3	75.1	54.9	18.4
+ 2D Img. Filtering w/ DINO	50.7	76.8	59.1	19.1
BEVFusion (RGB + LiDAR)	45.5	75.5	52.0	12.8

B. Inference Runtime

We compare the inference runtime of our method against prior works on a single A100 GPU (with a batch size of 1)

Table 7. **Inference Timing Results.** We find that our proposed approach is often faster than existing state-of-the-art methods. Since our late-fusion approach requires running two uni-modal detectors, we can speed up inference by running these in parallel. Notably, our fusion approach is light-weight and requires minimal overhead at inference.

	FCOS3D	BEVFormer	CP	TransFusion	DeepInteraction	CP+FCOS3D	Ours
	[57]	[34]	[64]	[2]	[65]	[42]	
Speed (ms)	89	327	323	367	590	324	323

Table 8. **NDS Results.** We compare methods reported in the main paper w.r.t nuScenes Detection Score (NDS) and mAP. We find that methods follow the same rankings on both metrics.

	FCOS3D	BEVFormer	CP	TransFusion	DeepInteraction	CMT	CP+FCOS3D	Ours
	[57]	[34]	[64]	[2]	[65]	[64]	[42]	
mAP	20.9	27.3	39.2	39.8	43.7	44.4	43.6	51.4
NDS	30.4	38.8	54.9	53.9	54.4	55.9	56.7	60.4

in Table 7, following the protocol described in [43]. As uni-modal RGB and LiDAR detectors run in parallel, the overhead of score calibration and fusion is negligible. Our method has the same runtime as CenterPoint (CP), and is faster than TransFusion [2], BEVFormer [34] and DeepInteraction [65].

C. AP vs. NDS Results

We report nuScenes Detection Score (NDS) and mAP results in Table 8. We find that all prior methods follow the same ranking on both metrics. This is unsurprising because NDS is computed as a weighted sum of mAP and other true positive metrics, where mAP is weighted five times greater than other components.

D. Results on Argoverse 2

We present results on the large-scale Argoverse 2 (AV2) dataset developed for autonomous vehicle research. AV2 evaluates on 26 classes, which follow a long-tailed distribution. Following [42], we train on and evaluate detections up to 50m. As shown in Table 9, our main conclusions from nuScenes still hold for AV2. FCOS3D yields poor performance on all classes, likely due to inaccurate depth estimates. CenterPoint performs considerably better, achieving high accuracy on classes with many examples. Notably, CenterPoint performs better on AV2’s rare classes (30.2 AP) compared to nuScenes’s rare classes (3.5 AP), likely because AV2 has more examples per-class in-the-tail. Lastly, our proposed late-fusion approach yields an 8.3% improvement over CenterPoint and a 3.9% improvement over prior

Table 9. **Comparison with the Argoverse 2 State-of-the-Art.**

We present results on AV2 evaluated at 50 meters. FCOS3D achieves poor performance, likely due to inaccurate depth estimates. In contrast, CenterPoint achieves strong performance on all classes. Our multi-modal fusion approach significantly improves over CenterPoint, achieving an 8.3% improvement averaged over all classes. These results on AV2 are consistent with those on nuScenes, demonstrating the general applicability of our approach.

Method	Modality	All	Many	Medium	Few
FCOS3D [57]	C	14.6	27.4	17.0	7.8
CenterPoint [66]	L	44.0	77.4	46.9	30.2
CenterPoint + FCOS3D [42]	C + L	48.4	79.0	51.4	35.3
Multi-Modal Late Fusion (Ours)	C + L	52.3	89.4	54.2	38.7

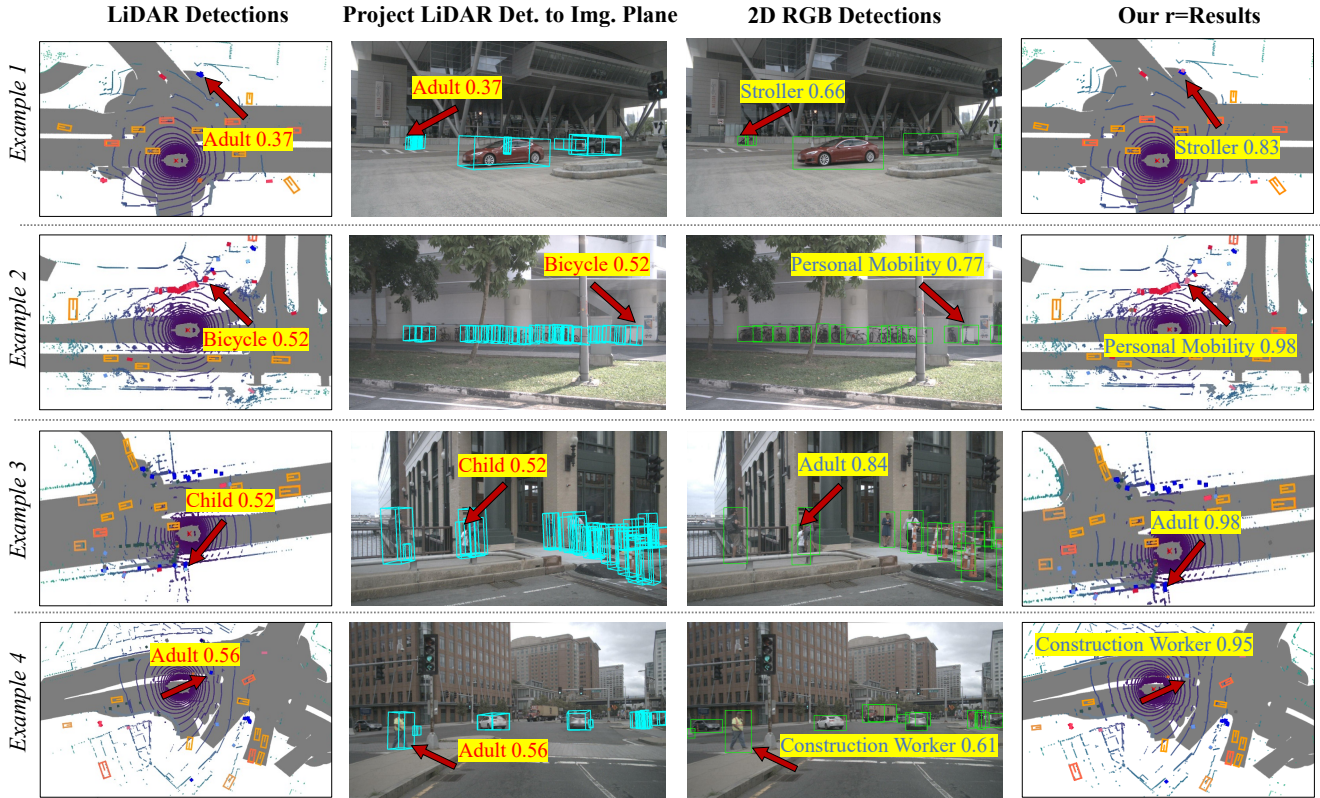


Figure 6. **Additional Qualitative Results.** We visualize the output of our late-fusion method which combines 3D LiDAR detections from CenterPoint and 2D RGB detections from DINO. In all cases, we find that the 2D RGB detector is able to correct classification errors from the 3D LiDAR detector, improving overall performance. Importantly, score calibration and probabilistic ensembling increases the confidence of the final prediction.

work. These new results on AV2 are consistent with those on nuScenes, demonstrating the general applicability of our approach.

E. More Visualizations

We present additional visualizations of our late-fusion approach in Fig. 6. Our method correctly classifies geometrically similar but semantically different categories like adult-vs-stroller, bicycle-vs-personal mobility, child-vs-adult, and adult-vs-construction worker.